Probabilistic Multi-Tensor Estimation Using The Tensor Distribution Function

Alex Leow, Siwei Zhu
University of California, Los Angeles

Katie McMahon, Greig I. de Zubicaray, Matt Meredith, Margie Wright
Functional MRI Laboratory, Queensland Institute of Medical Research and The University of Queensland

Paul Thompson
University of California, Los Angeles

Abstract

Diffusion weighted magnetic resonance (MR) imaging is a powerful tool that can be employed to study white matter microstructure by examining the 3D displacement profile of water molecules in brain tissue. By applying diffusion-sensitized gradients along a minimum of 6 directions, second-order tensors can be computed to model dominant diffusion processes. However, conventional DTI is not sufficient to resolve crossing fiber tracts. Recently, a number of high-angular resolution schemes with greater than 6 gradient directions have been employed to address this issue. In this paper, we introduce the Tensor Distribution Function (TDF), a probability function defined on the space of symmetric positive definite matrices. Here, fiber crossing is modeled as an ensemble of Gaussian diffusion processes with weights specified by the TDF. Once this optimal TDF is determined, the diffusion orientation distribution function (ODF) can easily be computed by analytic integration of the resulting displacement probability function.

1. Introduction

In the past decade, diffusion magnetic resonance imaging (MRI) has become a powerful tool for studying the structure of fibrous materials. By applying diffusion-sensitized gradients, diffusion MRI characterizes the particle diffusivity profile in various tissues. When the duration of the applied diffusion sensitization δ is much smaller than the time between the two pulses, the MR signal attenuation is related to the displacement probability function using a Fourier integral relationship with respect to a wave vector q [1].

In brain imaging, diffusion MRI is particularly advantageous over conventional non diffusion-weighted MRI as it can reveal the configuration and orientation of fiber tracts in white matter. The Diffusion Tensor MRI (DT-MRI) proposed in [2] models the water displacement probability function using a zero-mean 3D Gaussian distribution whose covariance matrix, a second-order positive-definite symmetric tensor, represents the principal directions of diffusion and orientation of local fiber tracts. Although extremely powerful and easy to compute, DT-MRI has some disadvantages. For example, any Gaussian probability distribution function has at most one orientational mode (principal direction), and thus can not resolve fiber crossing.

More recently, several different approaches have been developed to address this issue, involving sets of diffusion gradients with high angular resolution, by sampling the q-space on one or more shells with fixed radii. Methods such as the q-ball imaging technique [3], the Persistent Angular Structure (PAS) technique [4] and Spherical deconvolution techniques [5] have been proposed to recover partial information on the displacement probability function, while still allowing the inference of underlying fiber orientations.

In this paper, we propose a new approach, the computation of the tensor distribution function (TDF), to model fiber crossing in diffusion MR images. By using Gaussian distributions as basis functions, we expand the unknown displacement probability function with the weights given by the TDF. This may also be viewed as a natural, probabilistic extension of the multi-compartmental model. With the computation of the TDF, the water displacement probability function, orientation distribution function (ODF), tensor orientation distribution (TOD), and their corresponding anisotropy measures may all be obtained through simple analytic relations.

2. Theory

In standard diffusion-weighted MRI, images are acquired using the Stejskal-Tanner pulsed gradient spin-echo method. With some simplifications (rectangular pulse pro-

978-1-4244-2243-2/08/$25.00 ©2008 IEEE

files), measured image intensities S are linked to p, the displacement probability function of water molecules, via the following Fourier transform

$$S(q) = S(0) \int p(x) \exp(iq \cdot x) dx \tag{1}$$

here the wavenumber $q = r\delta G$, where r, δ, and G are the gyromagnetic ratio, the duration of the diffusion sensitization, and the applied magnetic gradient vector. Without loss of generality, let us assume the constant S(0) is 1.

Assuming a simple Gaussian-diffusion one-tensor model, the displacement probability function evaluated at position x (given diffusion tensor D, and diffusion time t) is

$$p(x) = ((4\pi t)^3 \det(D))^{-\frac{1}{2}} \exp\Big(- \frac{x^t D^{-1} x}{4t} \Big) \tag{2}$$

Thus, the measured diffusion MR image intensities in this one-tensor case is simply $S(q) = \exp(-tq^t Dq)$. It is often useful to use the normalization $\tilde{q} = q/|q|$, and the notation $b = t|q|^2$. In this case, we have $S(\tilde{q}) = \exp(-b\tilde{q}^t D\tilde{q})$.

2.1. The Tensor Distribution Function

Let us first denote the space of symmetric positive definite 3-by-3 matrices as $\mathbb{D}$. We seek a probabilistic ensemble of tensors, as represented by a Tensor Distribution Function P defined on the tensor space $\mathbb{D}$, that best explains the observed diffusion-weighted images. In this case, the calculated image intensity is

$$S_{calculated}(q) = \int_{D \in \mathbb{D}} P(D) \exp\Big(- tq^t Dq \Big) dD \tag{3}$$

To solve for an optimal TDF P^*, we apply multiple diffusion-sensitized magnetic field gradients in directions q_is, and arrive at P^* using the least-squares principle

$$P^* = \text{argmin}_P \sum_i \Big(S_{obs}(q_i) - S_{calculated}(q_i) \Big)^2 \tag{4}$$

To simplify our derivations, we define the error vector $E(q_i) = S_{obs}(q_i) - S_{calculated}(q_i)$ to be the contribution to the total error with respect to q_i. For $P(D)$ to be a true tensor distribution function, we have to enforce two contraints, i.e., the non-negativity constraint: $P(D) \geq 0$ for every D, and the probability density constraint: $\int P(D) dD = 1$.

To enforce the first constraint, we utilize the non-negativity property of the exponential function and let $P(D) = \exp(R(D))$. The minimization problem as proposed above is now optimized in the associated R space, ensuring the non-negativity of the resulting TDF. To this end, the gradient descent in the R space for this minimization problem is:

$$\frac{dR}{d\tau}(D) = \sum_i 2E(q_i) \exp(R(D)) F(D, q_i) \tag{5}$$

Here, τ is an artificial time, and $F(D, q_i) = \exp\big(- tq_i^t D q_i \big)$.

Let us now turn to address the second constraint. We first rewrite this constraint in the R space: $\int_{D \in \mathbb{D}} \exp\big(R(D)\big) dD = 1$, and modify the gradient direction in Eq.(5) by gradient projection onto the constraint space. This gives us the following modified gradient descent

$$\frac{dR}{d\tau}(D) = \sum_i E(q_i) \exp(R(D)) F(D, q_i) + \lambda \exp(R(D)) \tag{6}$$

where

$$\lambda = - \frac{\int_{D \in \mathbb{D}} \exp(R(D)) \sum_i E(q_i) \exp(R(D)) F(D, q_i) dD}{\int_{D \in \mathbb{D}} \exp(R(D))^2 dD}$$

2.2. Parametrizing the Tensor Space $\mathbb{D}$

The solution space $\mathbb{D}$ is a 6-dimensional space, and some reduction is necessary for numerical optimization. To this end, we assume that two eigenvalues (out of three) are equal for each individual tensor in $\mathbb{D}$, which is reasonable in practice. With this assumption, we only need to specify, for each tensor, one unit direction on the sphere which we associate with the third eigenvalue. Thus, each tensor is now represented by two scalars (specifying 3 eigenvalues) and one unit direction, allowing us to reduce $\mathbb{D}$ to a 4-dimensional space. In other words, every tensor D may be expressed using $D(\lambda, \theta)$, where the eigenvalues $\lambda = (\lambda_1, \lambda_2)$ (with λ_2 the repeated eigenvalue), and $\theta = (\theta_1, \theta_2)$ the azimuthal and polar angles associated with λ_1. Here we do not specify whether the two equal eigenvalues are smaller or greater than the third eigenvalue, allowing more types of tensors to be included.

Lastly, the unit direction associated with each tensor in $\mathbb{D}$ is initially expanded and parameterized with respect to the n diffusion-sensitized gradient directions q_is. The rationale behind this particular discretization is that the angular resolution of computed fiber tracts should be linearly related to the number of independent diffusion-sensitized gradients employed when acquiring HARDI. Once an initial solution is computed for the tensor distribution function, we further refine the angular resolution (beyond that given by the diffusion-sensitizing gradient directions) by using a multi-resolution scheme.

2.3. From TDF to ODF and Beyond

Once the optimal TDF is calculated, the displacement probability function p is simply:

$$p(x) = \int_{D\in\mathbb{D}} P(D)((4\pi t)^3 \det(D))^{-\frac{1}{2}} \exp\Big(-\frac{x^t D^{-1} x}{4t}\Big) dD \tag{7}$$

Moreover, the ODF can be analytically computed by radial integration:

$$\begin{aligned} ODF(\tilde{x}) &= C\int_{r=0}^{\infty} p(r\tilde{x})dr \\ &= C\int_{D\in\mathbb{D}} P(D)\Big(\det(D)\tilde{x}^t D^{-1}\tilde{x}\Big)^{-\frac{1}{2}} dD \end{aligned} \tag{8}$$

Here C is a normalizing constant. Lastly, we determine dominant fiber directions by examining the peaks in the Tensor Orientation Distribution Function (TOD), the marginal density function of the TDF by integrating out the eigenvalues $\lambda = (\lambda_1, \lambda_2)$:

$$\text{TOD}(\theta) = \int_{\lambda} P(D(\lambda,\theta))d\lambda \tag{9}$$

Once the dominant fiber direction θ^* is determined, one can estimate anisotropy measures (i.e., eigenvalues) of the dominant fibers (λ^*) by computing the expected values of λ along this direction.

$$\lambda^* = \frac{\int P(D(\lambda,\theta^*))\lambda d\lambda}{\int P(D(\lambda,\theta^*))d\lambda} \tag{10}$$

Here, we note that computing TOD may be advantageous when comparing our TDF approach to methods such as Q-ball imaging, where determination of dominant fiber tract directions is less straightforward.

2.4. Exponential isotropy via Shannon entropy

To provide a complete recipe for the TDF framework, here we seek a measure, similar to fractional anisotropy or generalized fractional anisotropy, that quantifies the overall anisotropy of any given voxel. First, we observe that the Shannon entropy (H) of any TDF P measures the randomness of this probabilistic ensemble, and thus inversely measures how certain we can estimate dominant fibers.

$$\text{H}(P(D)) = -\int_{D\in\mathbb{D}} P(D) log P(D) dD \tag{11}$$

In other words, here the Shannon entropy measures the isotropy of any given voxel, and thus we propose the exponential isotropy (EI) as follows.

$$\text{EI}(P(D)) = e^{-\int_{D\in\mathbb{D}} P(D) log P(D) dD} \tag{12}$$

Notice that unlike FA or GFA, EI takes greater values in white matter than in gray matter.

3. Results

In this section, we present experimental results to validate the proposed TDF approach. Two diffusion-sensitized gradient protocols were acquired from an individual subject on a Bruker Medspec 4 Tesla MRI scanner, with a transverse electromagnetic (TEM) headcoil. The timing of the diffusion sequence was optimized for SNR according to the scheme proposed in [6].

The first protocol used 27 diffusion-sensitized gradient directions, evenly distributed on the hemisphere, and three baseline scans with no diffusion sensitization (i.e., T2-weighted images). Acquisition parameters were (b-value: 1146 s/mm^2; TE/TR: 91.7/6090 msec; FOV=230x230; in-plane resolution: 1.8mmx1.8mm; 21 x 5mm slices with a 0.5mm gap; acquisition time 3:05 minutes). The second protocol used 94 diffusion-sensitized gradient directions, and 11 baseline scans with no diffusion sensitization (b-value: 1159 s/mm^2; TE/TR: 92.3/8250 msec; FOV=230x230; in-plane resolution: 1.8mmx1.8mm; 55 x 2mm contiguous slices; acquisition time 14:30 minutes). To assess the performance of the TDF approach, we first simulate various configurations of one-tensor systems using different b values and signal-to-noise ratios (SNR) (similar to those seen in real HARDI data). To quantitatively compare the proposed TDF approach to other methods in the literature, we compare the calculated ODF (from the computed TDF) and the true ODF using the L1-norm, L2-norm, and the Kullback-Leibler distance. Here, we chose $\lambda_1 = 18$ and $\lambda_2 = 2$ ($10^{-10} m^2 s^{-1}$) as the eigenvalues for each individual tensor, and employed Rician noise in our simulations. The ODFs were rendered using 642 points, as determined using an icosahedral approximation of the sphere.

Table 1 compares the mean and standard deviation of the three performance measures with a fixed b value and different SNR's (10, 15, and 20) using the 27-direction protocol. The results indicate that the TDF approach is robust, and is relatively independent of the SNR (signal-to-noise ratio). Moreover, the results are comparable to those reported in [5]. In Tables 2 and 3, we investigated the influence of b values on the performance measures, and the results indicated that the TDF approach, similar to other methods, performs better with increasing b values (in this paper, b ranges from 1000 to 4000 s/mm^2). To assess the performance in resolving fiber-crossing, we simulated two-tensor systems with equal weights and varying angles of crossing (45, 60 and 90 degrees), and the corresponding Kullback-Leibler distance measures are shown in Table 4. Typical examples of recovered ODFs are shown in Figure 1.

To compare the two acquisition protocols, similar 2-tensor simulations were conducted using the 94-direction protocol and the results are shown in Table 4 (here, b value and SNR are 1200 s/mm^2 and 15). Interestingly, the results indicate that the 27-direction protocol performs comparable

to the 94-direction protocol, indicating the numerical stability of both the TDF approach and the acquisition processes.

In the next experiment, we investigated the concept of the tensor orientation distribution function (TOD) by simulating 2-tensor systems with 90-degree crossing using the 94-direction protocol (the two tensors are: $10^{-10}diag(18,2,2)m^2s^{-1}$ and $10^{-10}diag(2,18,2)m^2s^{-1}$). Examples of computed TOD's are plotted at the bottom of Figure 1. Visually, we observe that the recovered TOD has two peaks corresponding to the true fiber orientations. To help visualize the recovered ODF's, two fiber bundles crossing at 90 degrees were simulated, using similar parameter settings as above, in a 10 by 10 by 1 grid (Figure 3). Notice that the fiber crossing is visually clearly resolved. In this case, the mean angular separation of the two recovered tensors, as computed using the corresponding TODs, is 89.8 degrees with a standard deviation of 4.3 degrees (in Fig. 2, we plotted the recovered dominant fiber orientations, using the spherical coordinate system, relative to the actual orientations used to simulate these 2-tensor systems).

To validate the TDF approach using real imaging data, the diffusion-weighted MR images of a normal control subject were acquired using the 27-direction acquisition protocol. Three regions were used (Fig. 7): region one covered the crossing of the corona radiata and corpus callosum; region two was obtained from the fanning of the arcuate fasciculus; region three from the corpus callosum where interhemispheric connections are known. The results are shown in Figs. 4-6. In these cases, the recovered ODF plots appear consistent with known anatomical structures. Lastly, the exponential isotropy (EI) plot for region one is shown in Fig. 8, illustrating the value of EI as a natural isotropy measure for the TDF approach.

4. Conclusion

In this paper, we introduced the computation of the Tensor Distribution Function (TDF) as a novel method to resolve intravoxel fiber crossing in HARDI. We presented mathematical formulations of the TDF, and proposed a projected gradient descent algorithm for numerical computation of TDF. With minor constraints on the diffusion process and the anisotropy of individual tensors, the proposed approach solves for an underlying tensor ensemble that best describes the observed diffusion-weighted MR images. Moreover, it offers some advantages relative to other methods since the displacement probability function, orientation distribution function, and principal fiber directions (or the tensor orientation function) may all be directly derived from TDF through simple analytic relations.

Table 1. Means and standard deviations (in parenthesis) of the three performance measures for one-tensor simulation results with varying SNR, $b = 1200s/mm^2$

SNR	10	15	20
KL	.0020 (1.1e-4)	.0022 (1.0e-4)	.0023 (6.2e-5)
L1	7.6e-4 (1.7e-5)	8.2e-4 (1.8e-5)	8.8e-4 (1.9e-5)
L2	.0032 (9.5e-5)	.0034 (3.5e-5)	.0035 (3.1e-5)

Table 2. Mean of the three performance measures for one-tensor simulation results with varying b, SNR = 15

b	1000	1500	2000	2500	3000	3500	4000
KL	0.0022	0.0022	0.0021	0.0019	0.0018	0.0014	0.0013
L1	8.2e-4	8.2e-4	7.6e-4	7.6e-4	7.0e-4	6.4e-4	5.7e-4
L2	0.0034	0.0034	0.0033	0.0032	0.0030	0.0027	0.0026

Table 3. Estimated standard deviation of the three performance measures for one-tensor simulation results with varying b, SNR = 15

b	1000	1500	2000	2500	3000	3500	4000
KL	1.2e-4	5.2e-5	8.7e-5	7.8e-5	7.9e-5	2.2e-4	1.4e-4
L1	6.4e-5	6.3e-4	6.0e-4	6.0e-4	5.5e-4	5.9e-5	3.9e-5
L2	1.1e-4	3.5e-5	7.1e-5	7.0e-5	7.2e-5	2.1e-4	1.4e-4

Table 4. Mean (and standard deviation) of KL distance for two-tensor simulation results with varying angles, $b = 1200s/mm^2$, SNR = 15

Angle	45	60	90
27 directions	2.5e-3 (4e-4)	4.0e-3 (4.5e-4)	3.4e-3 (5e-4)
94 directions	2.51e-3 (2.21e-4)	3.75e-3 (5.72e-4)	3.12e-3 (4.21e-4)

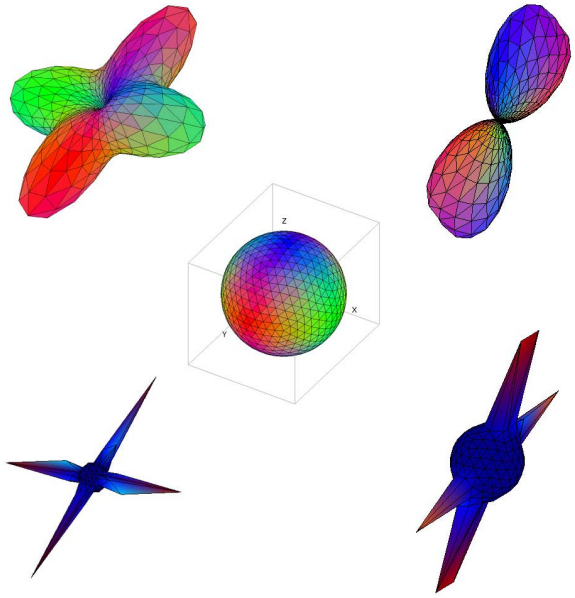

Figure 1. **Top:** Examples of typical recovered ODFs for a two-tensor system with relative orientations of 90 (left), and 60 (right) degrees (simulated data with 94 diffusion-sensitizing gradients, $b = 1200s/mm^2$, and SNR = 15). In these examples, we used the multi-grid method to refine angular resolution beyond the original 94 directions. Here, the final angular resolution is given by an icosahedral approximation of the sphere (642 directions). **Center:** A sphere showing the directional color coding used for the ODFs. **Bottom:** Recovered TOD of the same 2 systems.

References

[1] Stejskal, E. O. and Tanner, J. E. "Spin diffusion measurements: spin echoes in the presence of a time-

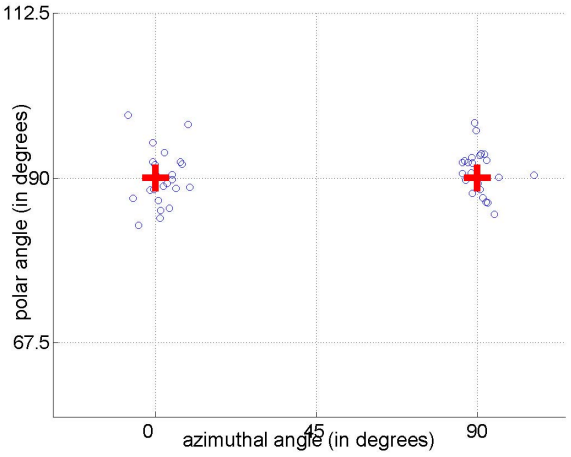

Figure 2. Recovered principle fiber directions, plotted using the azimuthal angle (x axis) and polar angle (y axis), of simulated 2-tensor systems (crossing at 90 degrees) as shown in Fig. 3. Here, principle directions are determined using the tensor orientation distribution function (the orientations of the two tensors used to simulate fiber crossing are marked in red).

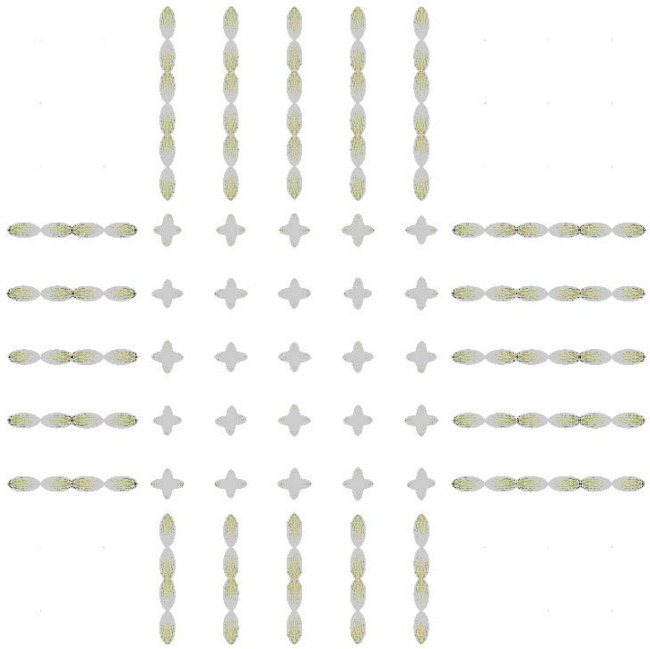

Figure 3. Recovered ODF plot for simulated 2-tensor crossing at 90 degrees using the 27-direction protocol (Rician noise; SNR = 15).

dependent field gradient." *J. Chem. Phys.* 42, 288-292, 1965

[2] Basser, P. J. "Inferring microstructural features and the physiological state of tissues from diffusion-weighted images." *NMR Biomed* 8, p. 333-344, 1995.

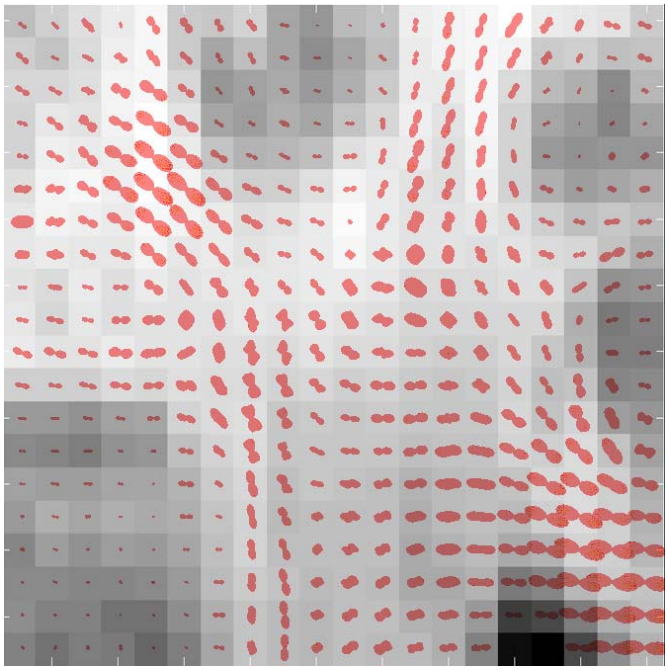

Figure 4. Recovered ODF plot from area 1 of the HARDI data in Fig. 7.

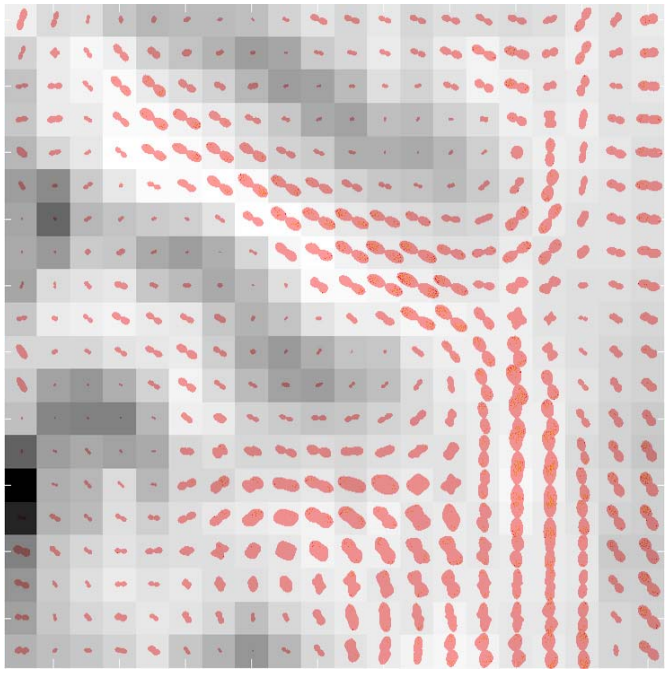

Figure 5. Recovered ODF plot from area 2 of the HARDI data in Fig. 7.

[3] Kalvis M Jansons and Daniel C Alexander. "Persistent Angular Structure: New Insights from Diffusion Magnetic Resonance Imaging Data." *Inverse Problems* 19, p. 1031-1046, 2003.

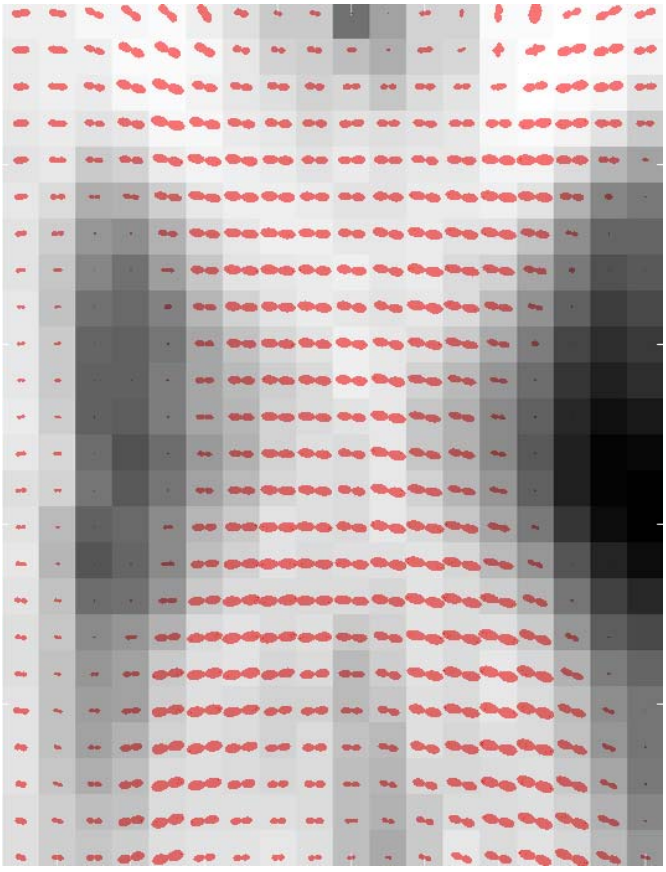

Figure 6. Recovered ODF plot from area 3 (Corpus Callosum) of the HARDI data in Fig. 7.

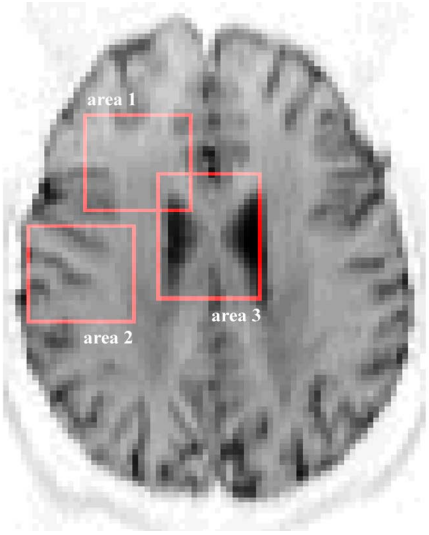

Figure 7. Positions of the windowed areas, in previous figures, with respect to the HARDI of a normal subject (baseline T2 image shown). See text for more information.

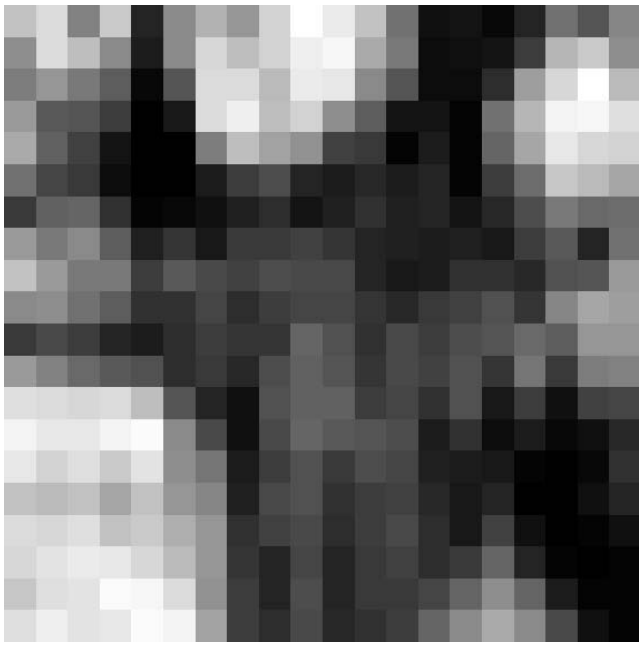

Figure 8. The exponential isotropy (EI) plot of Area 1 of the HARDI data in Fig. 7 (the corresponding ODF and GFA plot is shown in Fig. 4). Here, gray matter appears to have higher EI values than White matter.

[4] J-Donald Tournier, Fernando Calamante, David Gadian, and Alan Connelly. "Robust Determination of the Fiber Orientation Distribution in Diffusion MRI: Non-negativity Constrained Super-resolved Spherical Deconvolution." *NeuroImage* 35, p. 1459-1472, 2007.

[5] David S. Tuch. "Q-Ball Imaging." *Magnetic Resonance in Medicine* 52, p. 1358-1372, 2004.

[6] Jones, D.K., Horsfield, M.A., Simmons, A. "Optimal strategies for measuring diffusion in anisotropic systems by magnetic resonance imaging." *Magn. Reson Med.* 42(3), p. 515-525, 1999.